Electronic Supplementary Material (ESI) for CrystEngComm.

Supporting Information

The use of biocompatible crystalline substrates for heterogeneous nucleation and polymorphic selection of indomethacin

Tharanga K. Wijethunga, Xingyu Chen, Allan S. Myerson and Bernhardt L. Trout*

Department of Chemical Engineering, Massachusetts Institute of Technology, 77 Massachusetts Avenue, Cambridge, Massachusetts 02139, United States.

S1. Initial powder patterns for substrates

L-glutamic acid – β form (GLU)

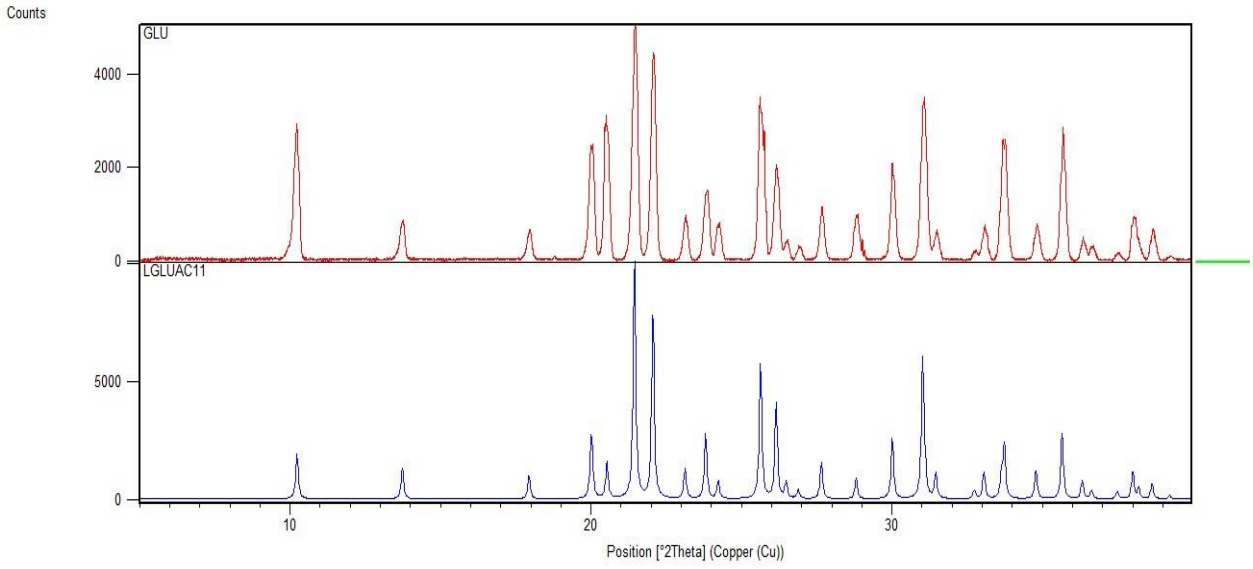

L-Threonine (THR)

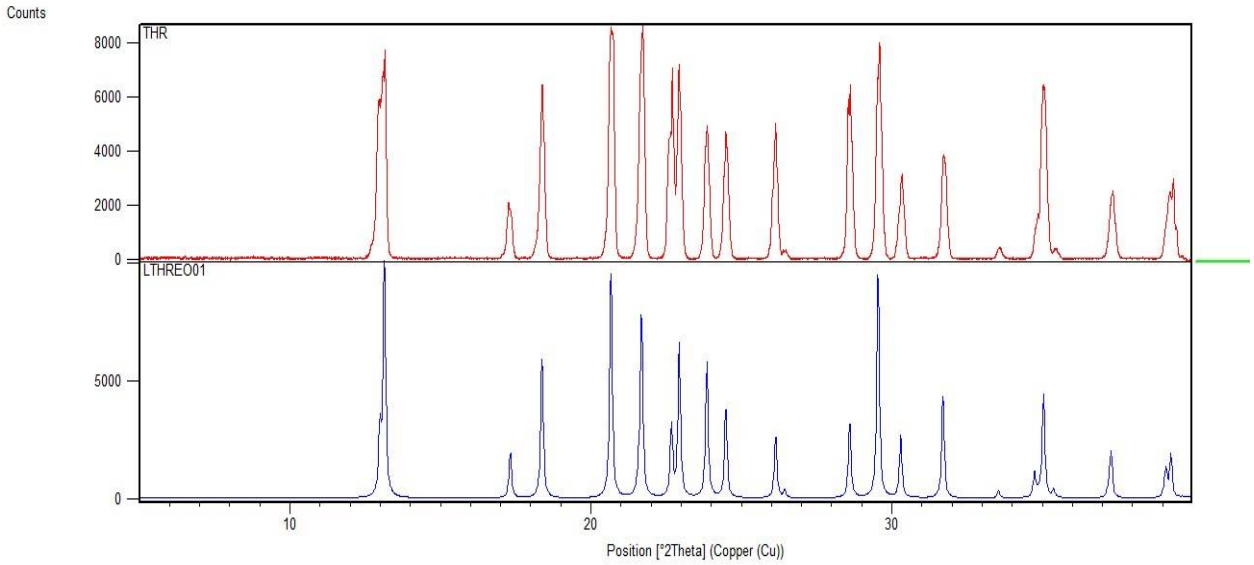

Allantoin (ALT)

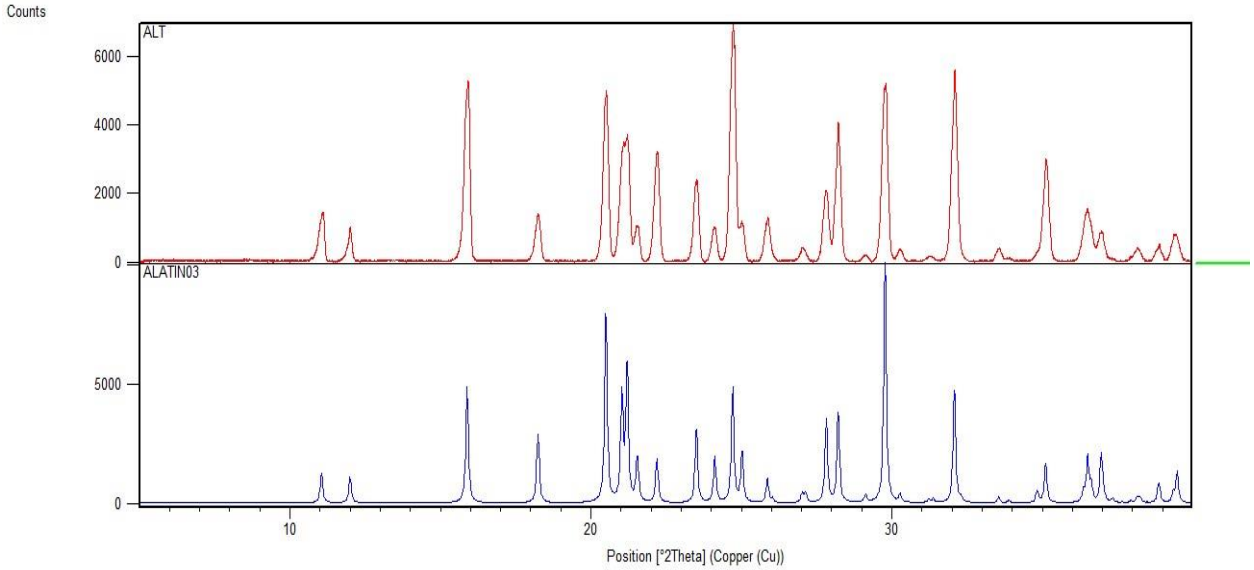

Xanthine (XAN)

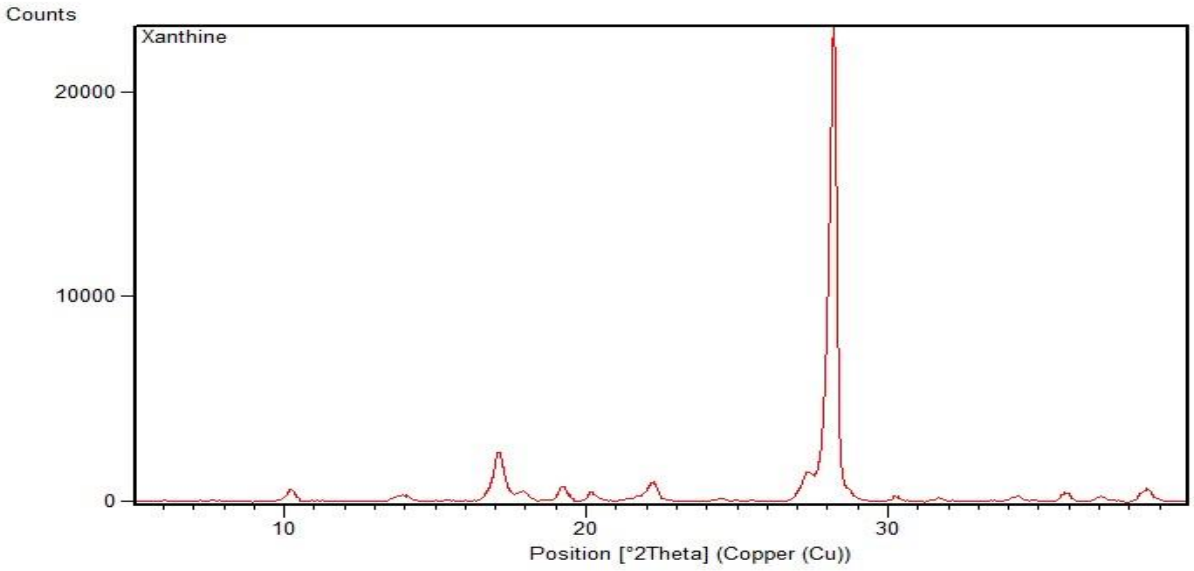

Biotin (BIO)

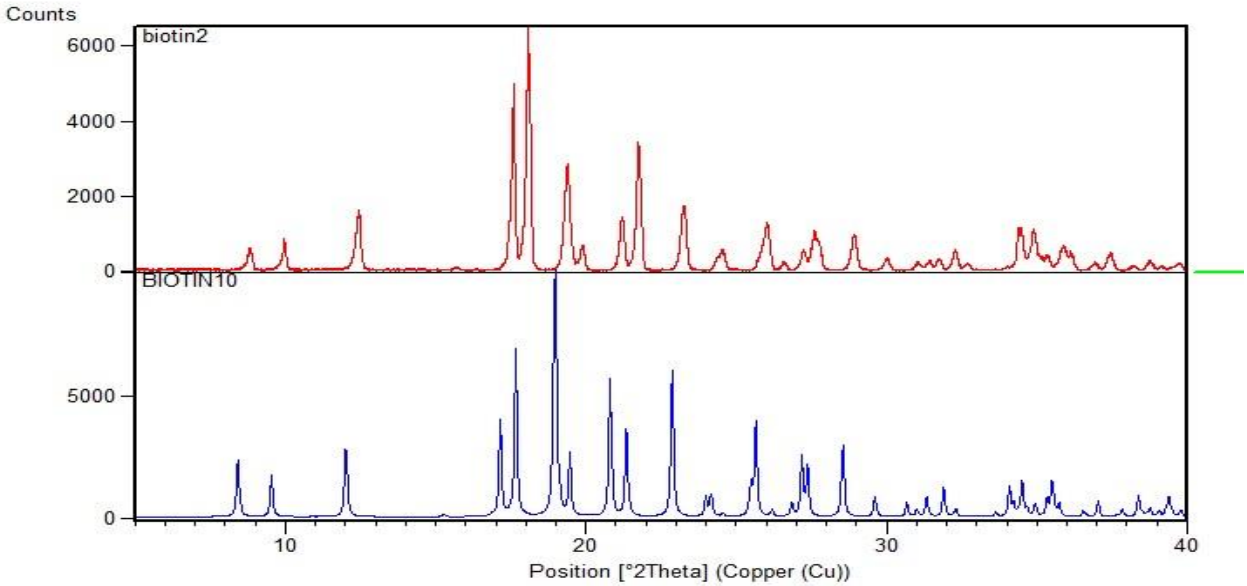

L-Histidine – Form A (HIS)

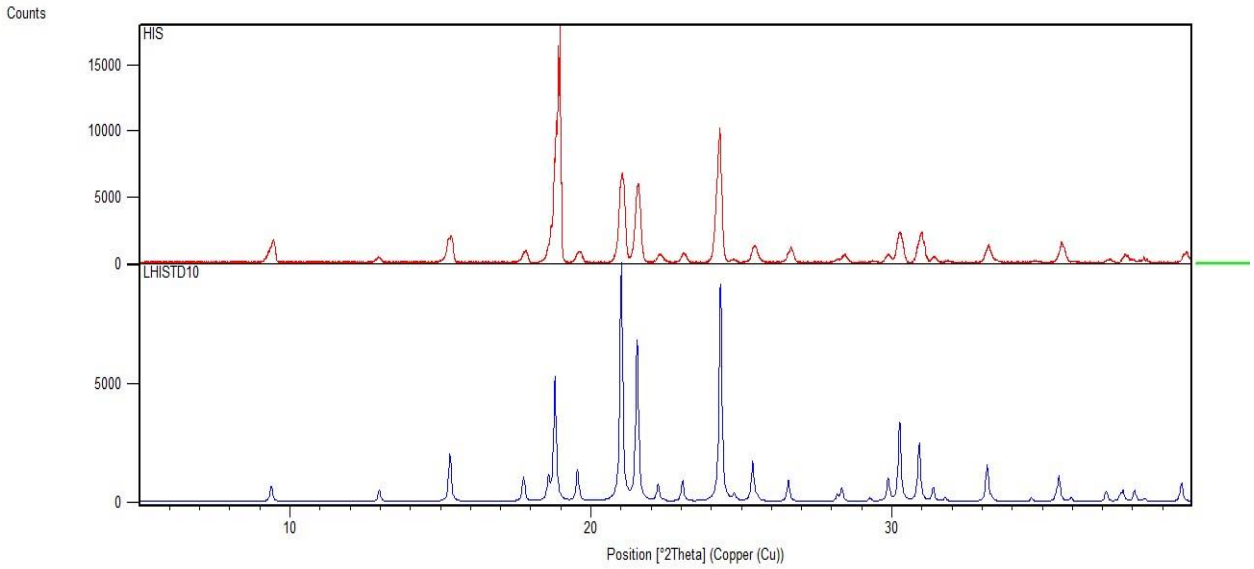

S2. Solubility of IMC in different solvents

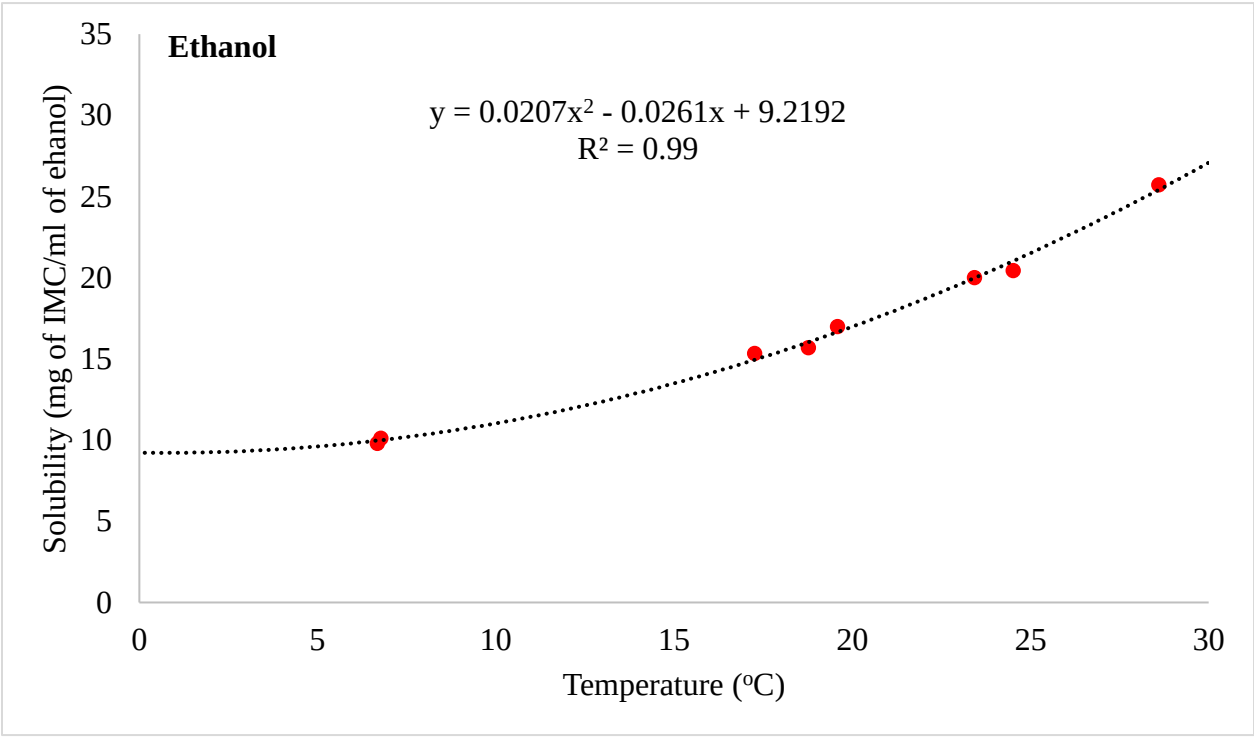

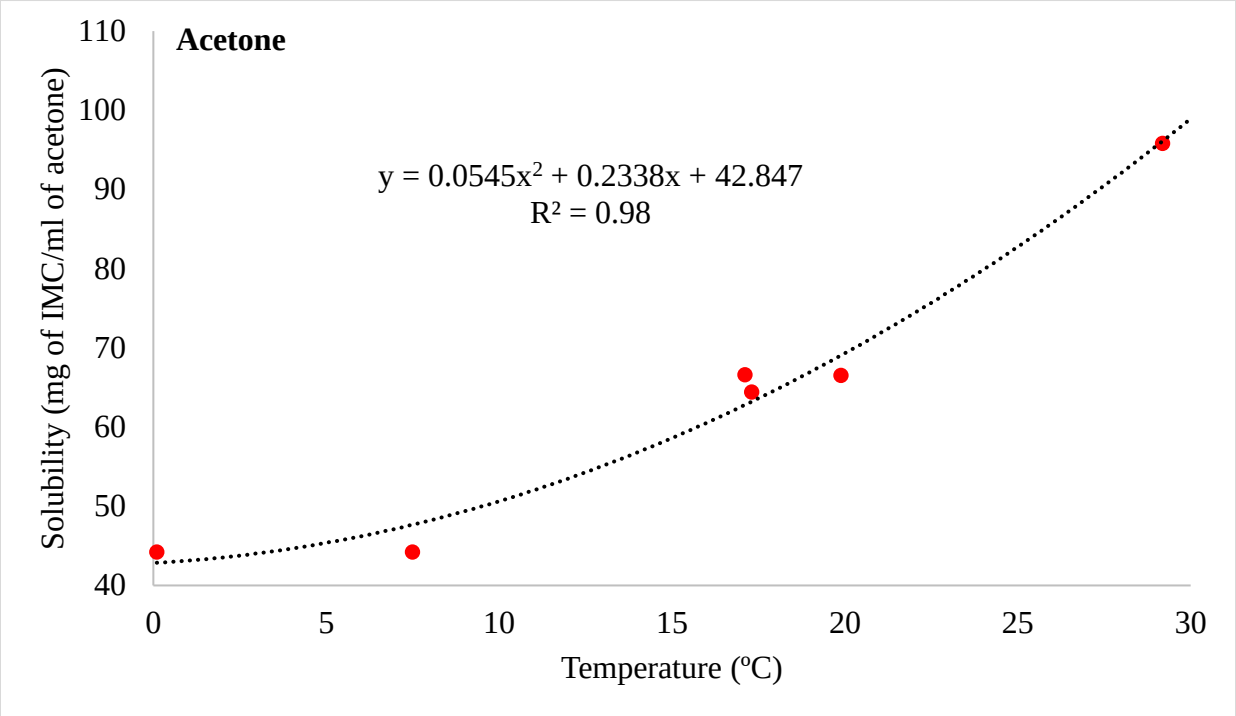
Acetone
y = 0.0545x² + 0.2338x + 42.847
R² = 0.98
Solubility (mg of IMC/ml of acetone)
Temperature (ºC)
110
100
90
80
70
60
50
40
0
5
10
15
20
25
30

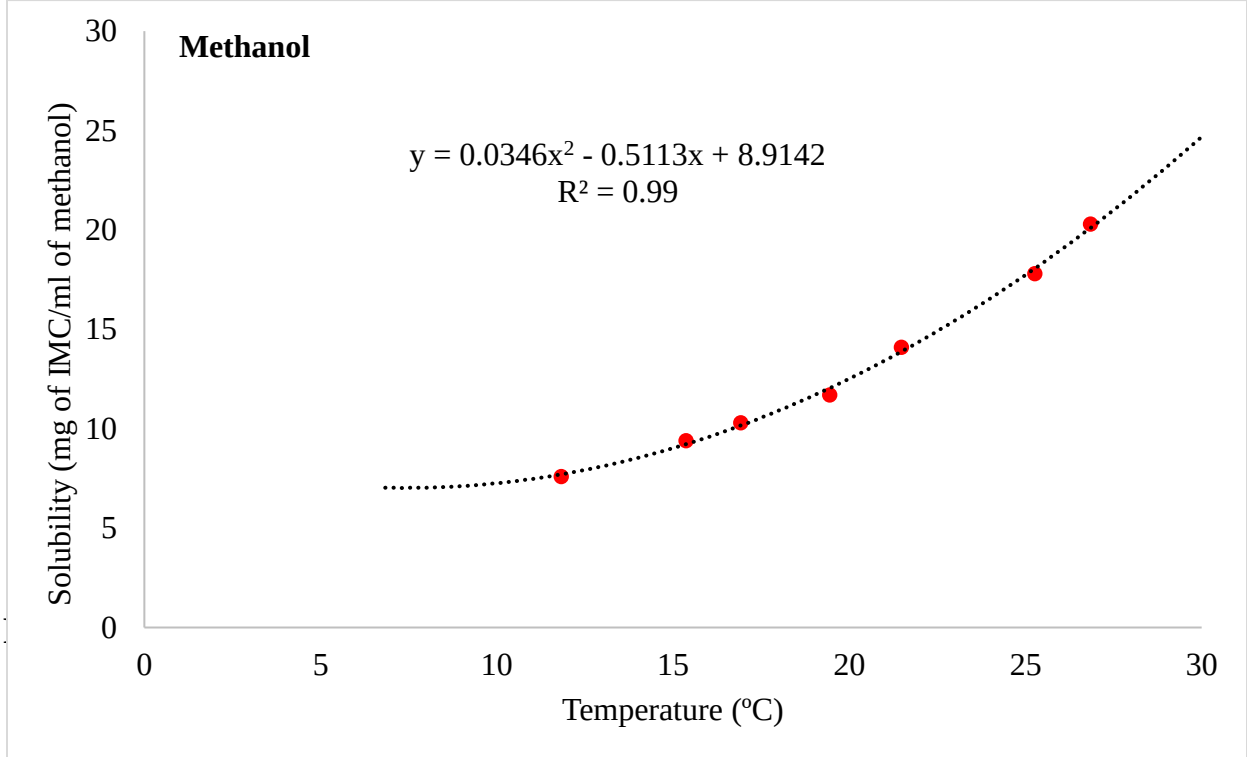
Methanol
y = 0.0346x² - 0.5113x + 8.9142
R² = 0.99
Solubility (mg of IMC/ml of methanol)
Temperature (ºC)
30
25
20
15
10
5
0
0
5
10
15
20
25
30

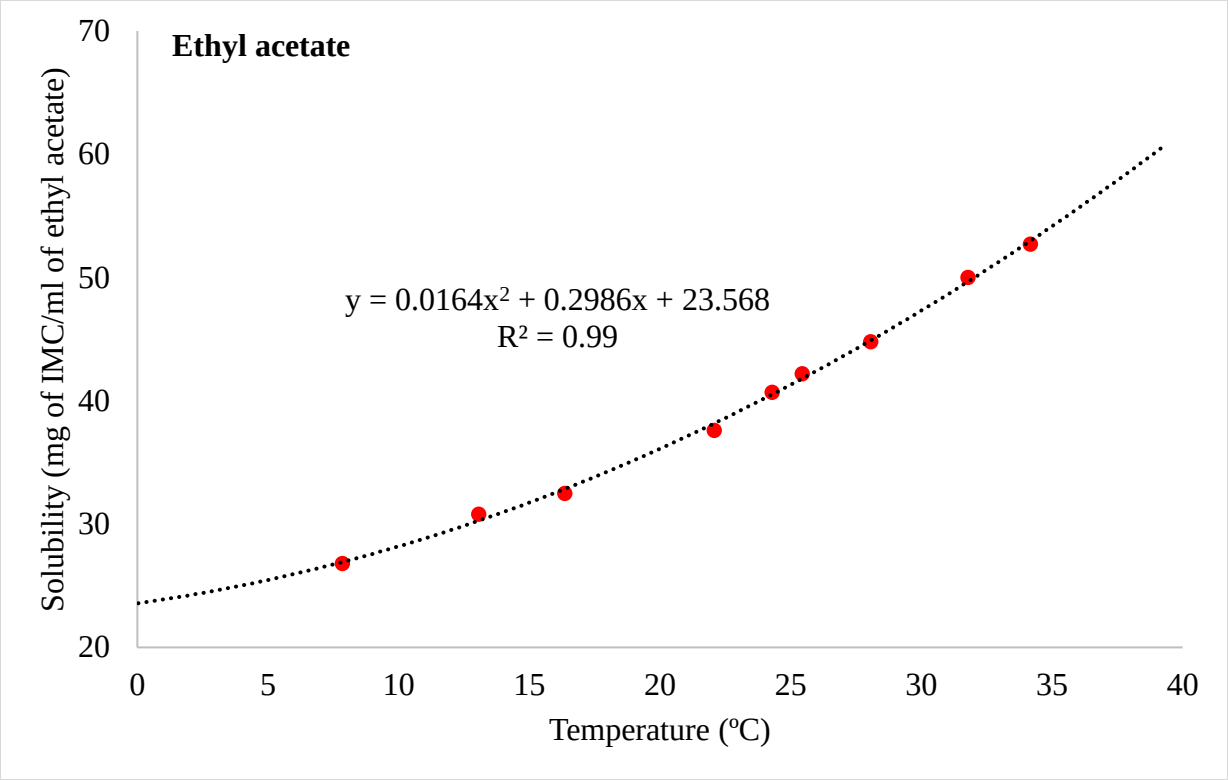
Ethyl acetate
Solubility (mg of IMC/ml of ethyl acetate)
y = 0.0164x² + 0.2986x + 23.568
R² = 0.99
Temperature (ºC)
70
60
50
40
30
20
0
5
10
15
20
25
30
35
40

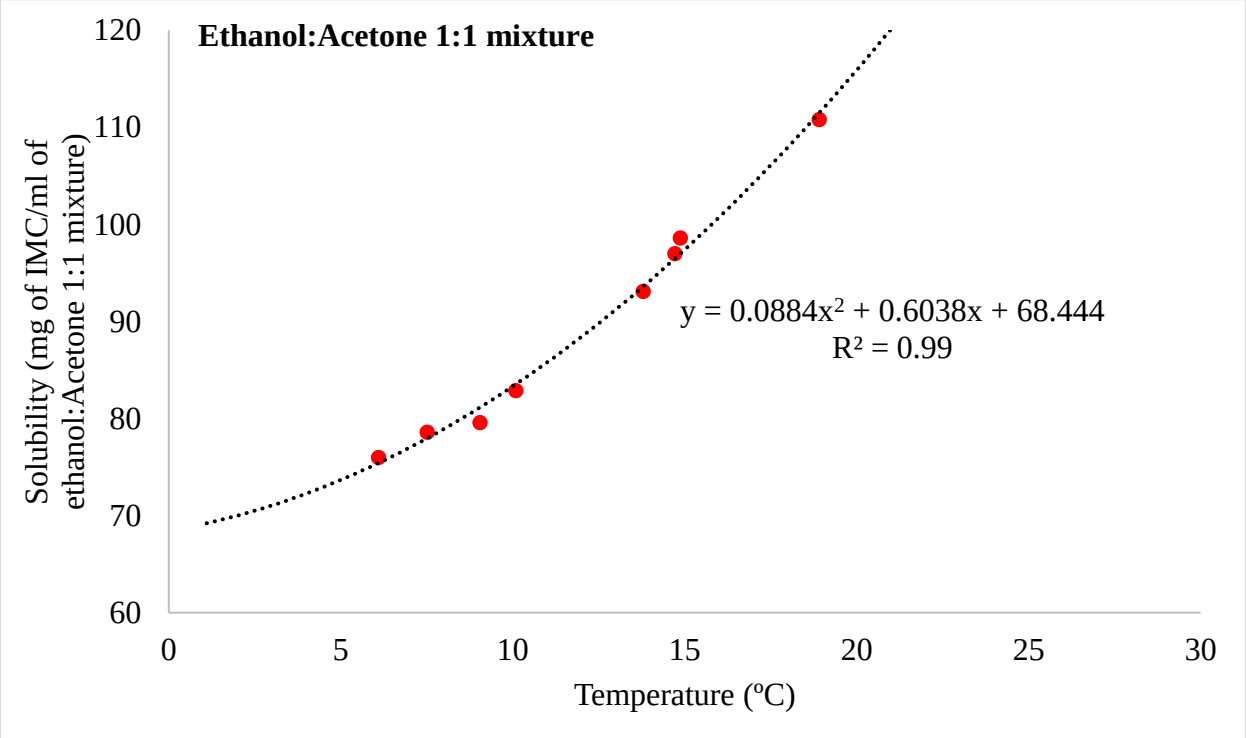
Ethanol:Acetone 1:1 mixture
Solubility (mg of IMC/ml of ethanol:Acetone 1:1 mixture)
y = 0.0884x² + 0.6038x + 68.444
R² = 0.99
Temperature (ºC)
120
110
100
90
80
70
60
0
5
10
15
20
25
30

S3. Microscopic setup used for high throughput induction time measurements

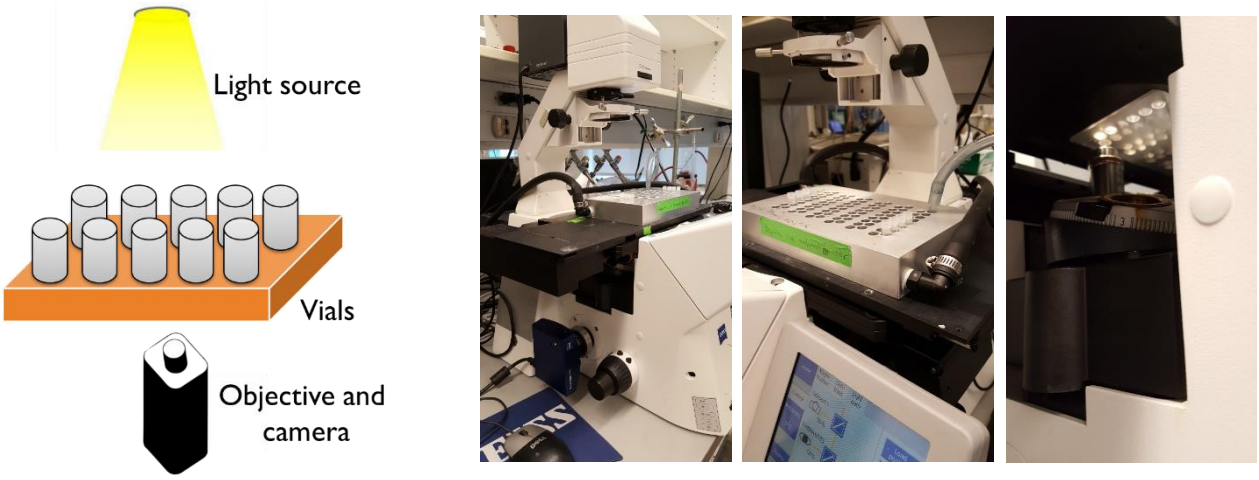

S4. Formation of IMC forms in the presence of HIS

Formation of a) γ-IMC and b) α-IMC attached to HIS crystals and their morphologies c) γ-IMC and d) α-IMC under light microscope

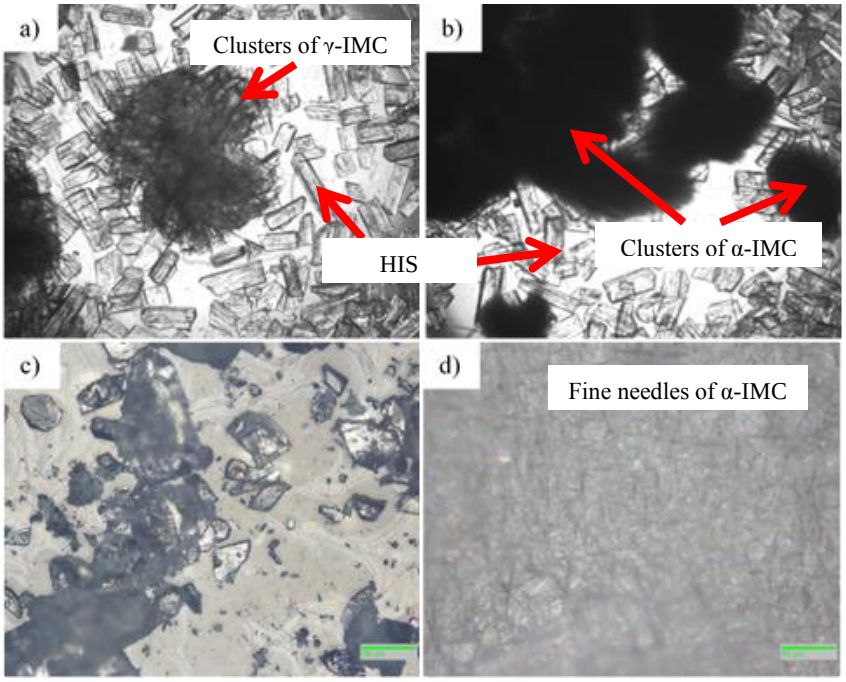

S5. PXRD patterns of IMC polymorphs

γ-form

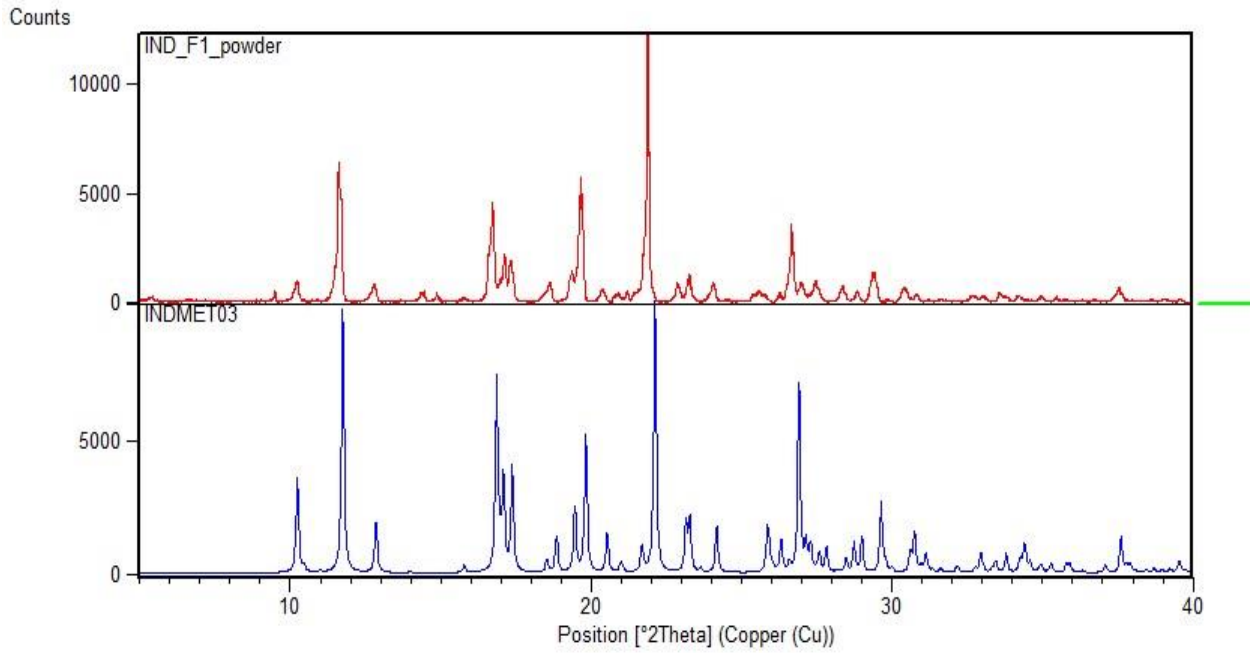

α-form

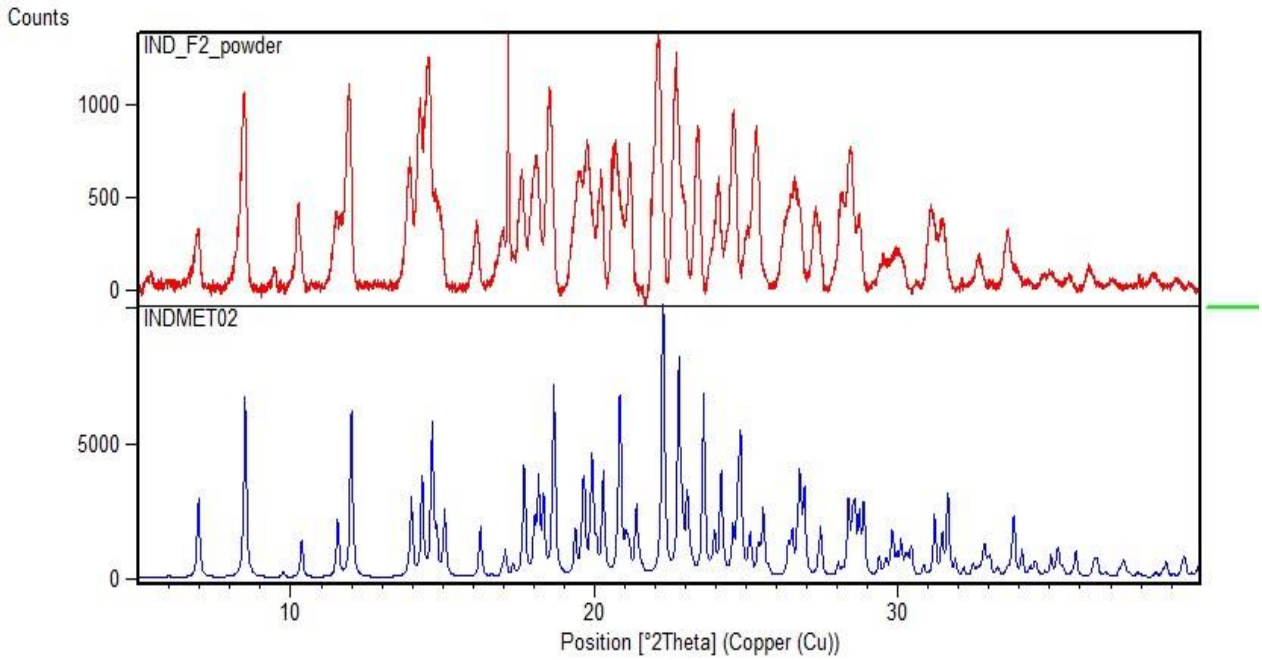

S6. Raman spectra of IMC polymorphs

γ-form

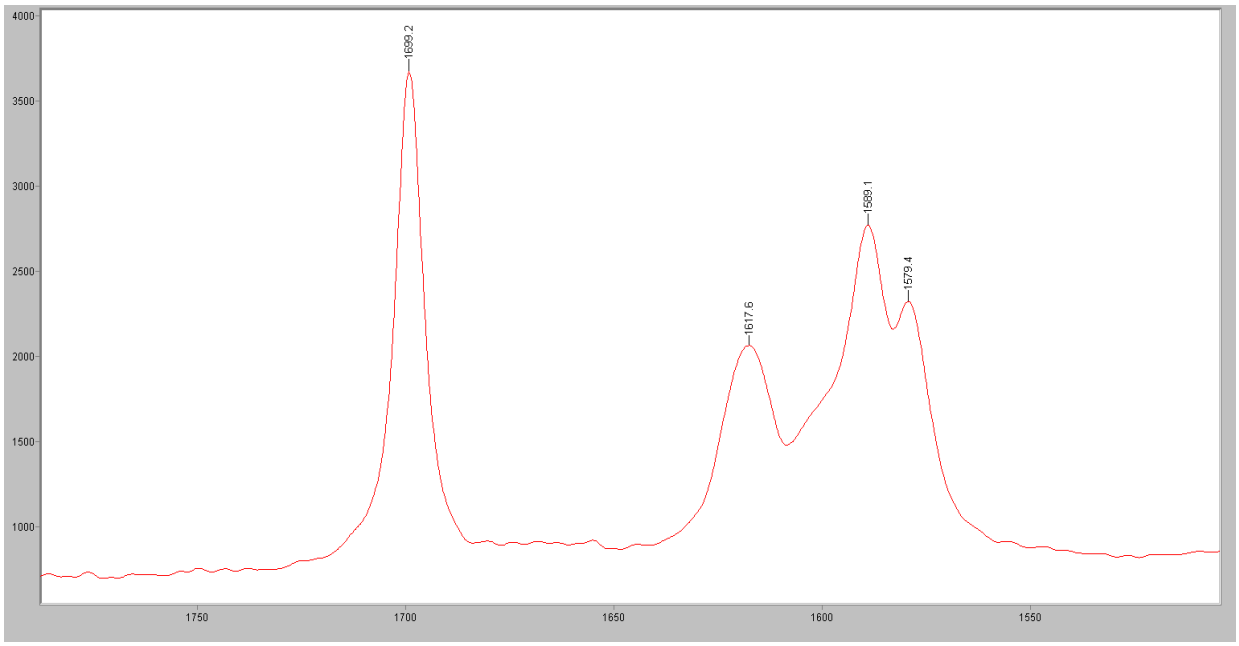

α-form

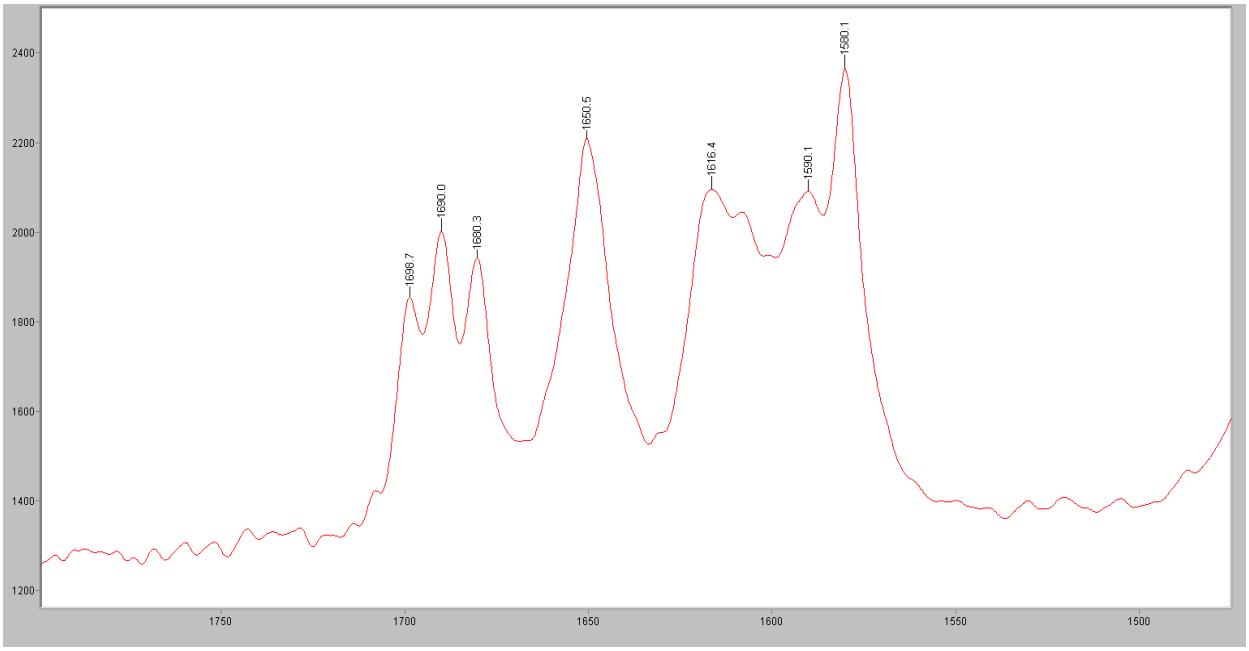

S7. Association energy calculations

Possible binding pockets on each substrate molecule

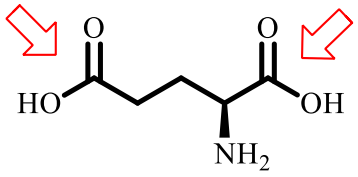

L-Glutamic acid (GLU)

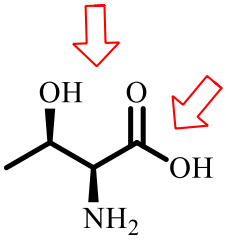

L-Threonine (THR)

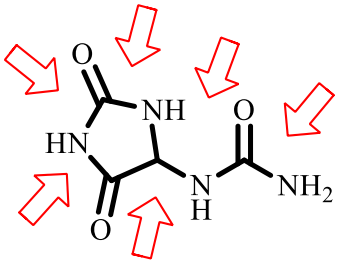

Allantoin (ALT)

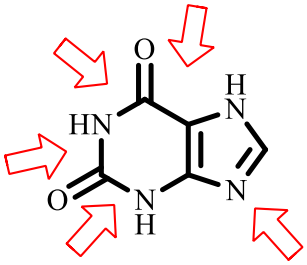

Xanthine (XAN)

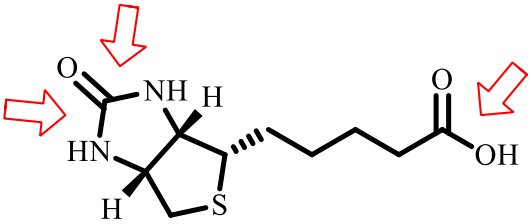

Biotin (BIO)

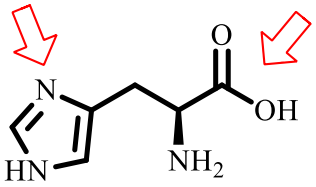

L-Histidine (HIS)

Minimized energies for optimized individual molecules and molecular pairs

Compound	Minimized energy (kcal/mol)
IMC	+50.29
GLU	-7.52
THR	+29.00
XAN	-162.02
HIS	+21.54
ALT	-227.56
BIO	-110.78
IMC: GLU	+18.77
IMC: THR	+57.86
IMC: XAN	-131.70
IMC: HIS	+47.98
IMC: ALT	-202.54
IMC: BIO	-84.76

Calculated association energies between IMC and substrates for the lowest energy pairs

Molecular pair	**ΔE (kcal/mol)**
IMC:ALT	-25.27
IMC:BIO	-24.27
IMC:THR	-21.43
IMC:HIS	-21.41
IMC:GLU	-20.38
IMC:XAN	-19.97

Possible binding modes between IMC and ALT (Energies are provided in kcal/mol)

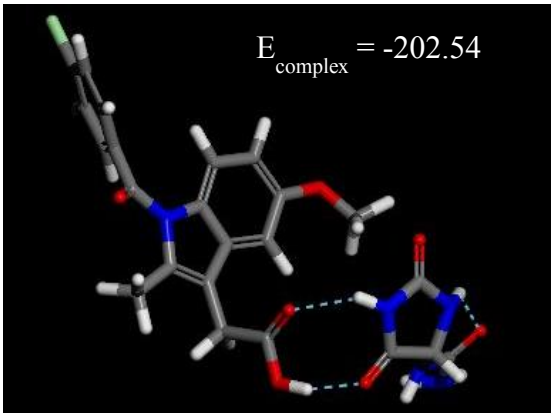

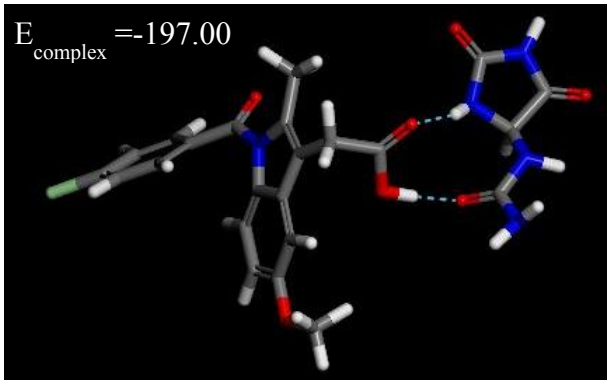

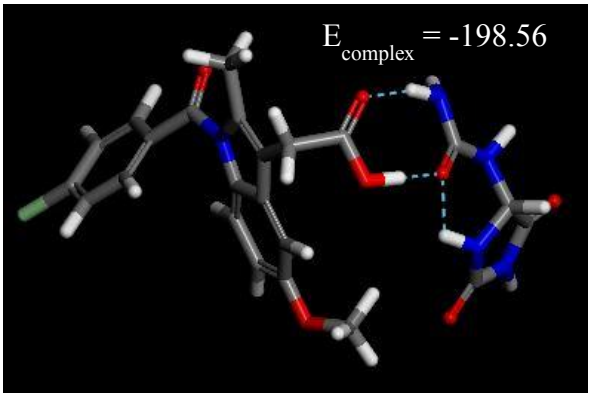

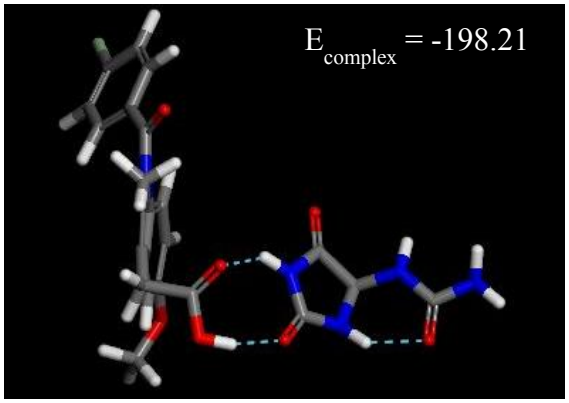

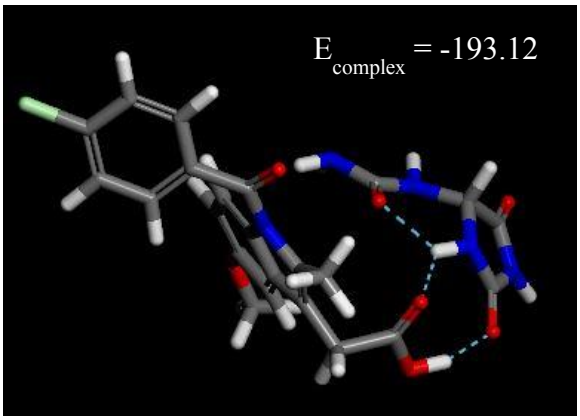

S8. Single crystals used for SCXRD and Raman library building

IMC – γ form

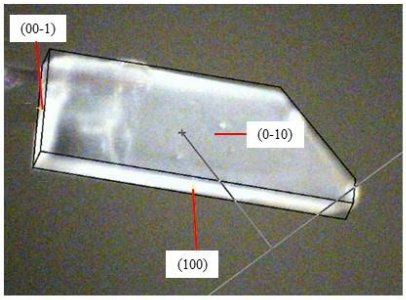

Crystal 1

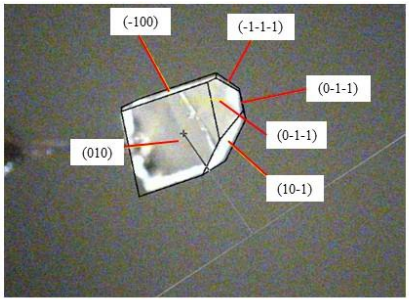

Crystal 2

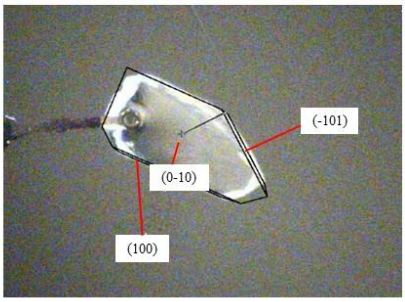

Crystal 3

HIS

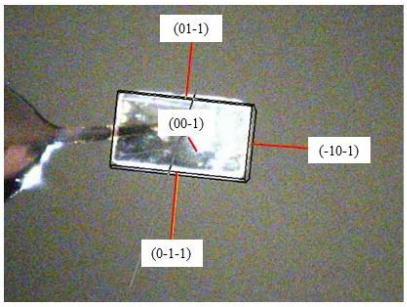

Crystal 1

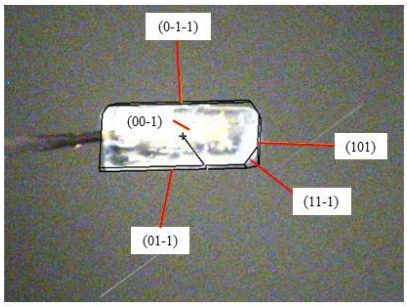

Crystal 2

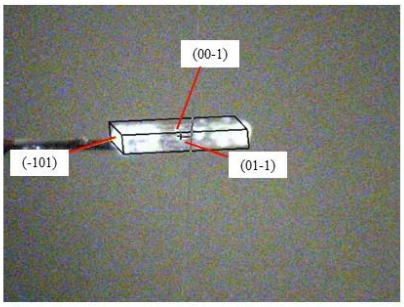

Crystal 3

GLU

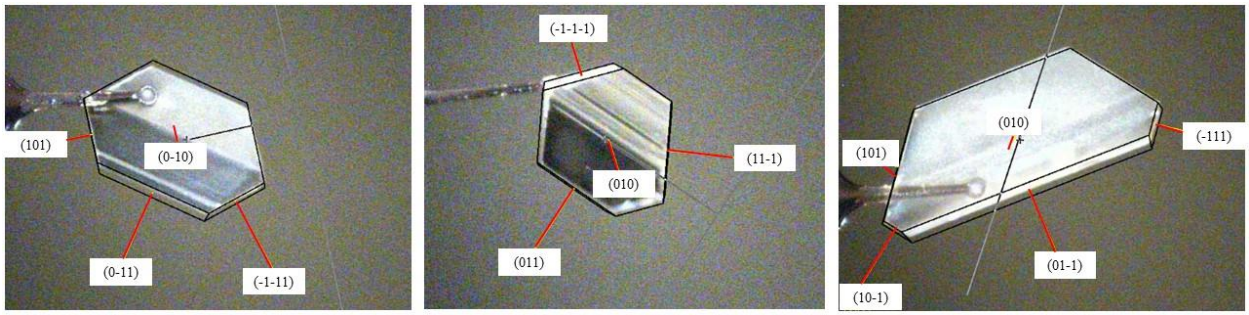

Crystal 1 Crystal 2 Crystal 3

S9. Induction experiments – full data sets for logarithmic fit

Overall nucleation of IMC

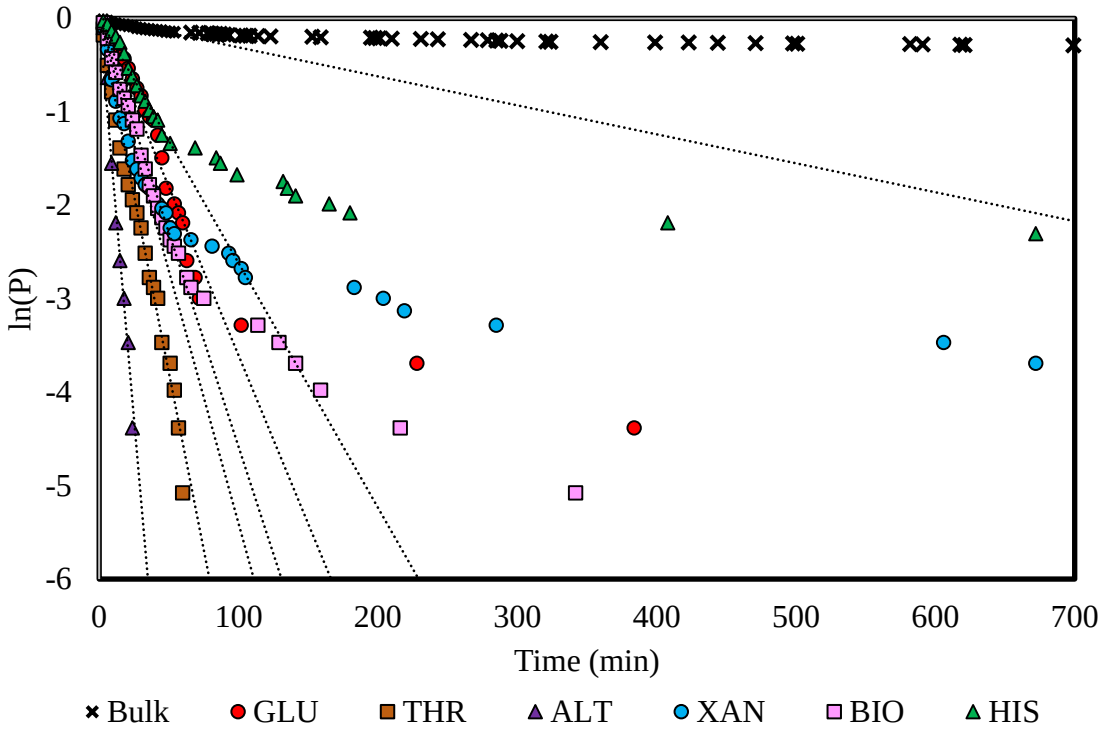

Nucleation of γ-from IMC

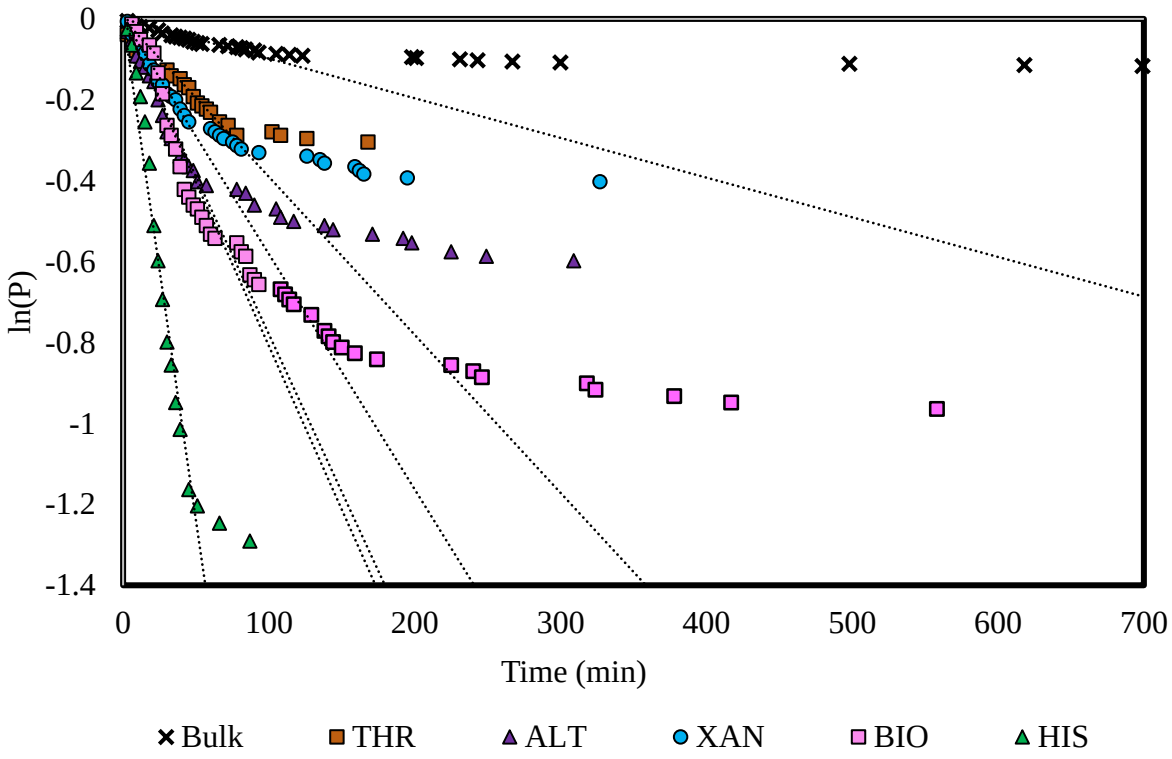

Nucleation of α-from IMC

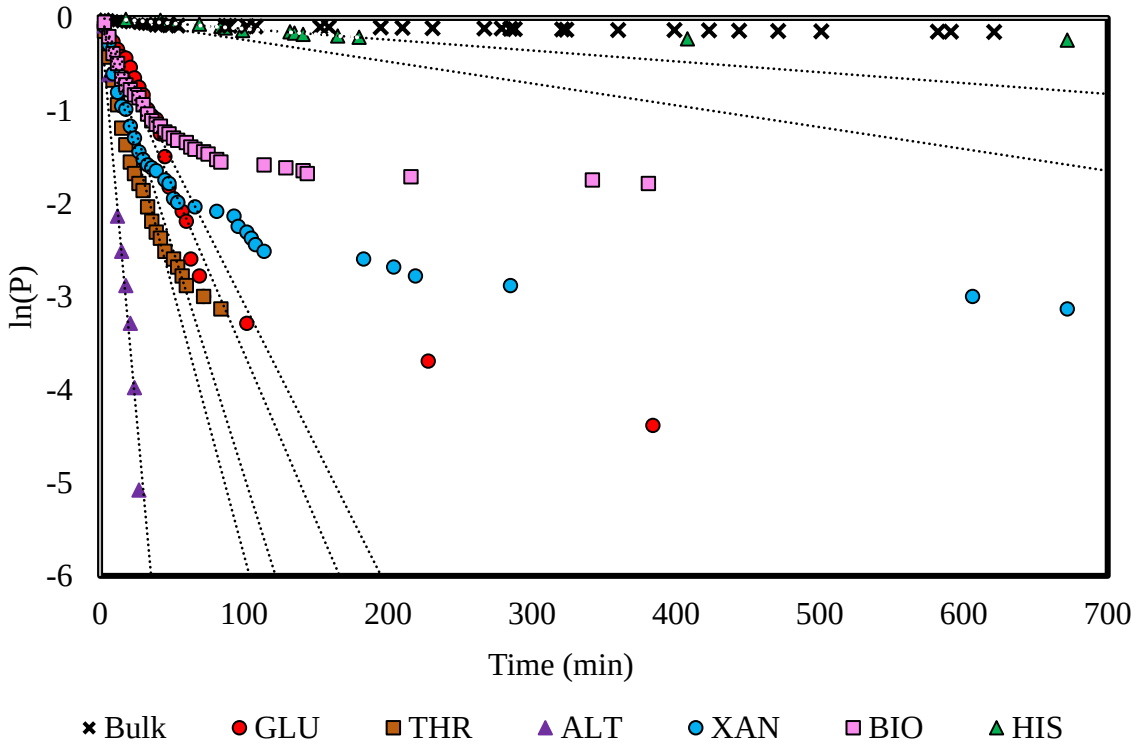

S10. Association energy calculations between IMC conformations, GLU and HIS

a) *Trans* and b) *cis* orientations of carboxylic acid and Cl functional groups in IMC γ- and α-form

a)

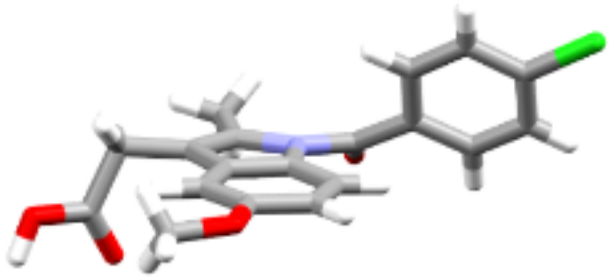

b)

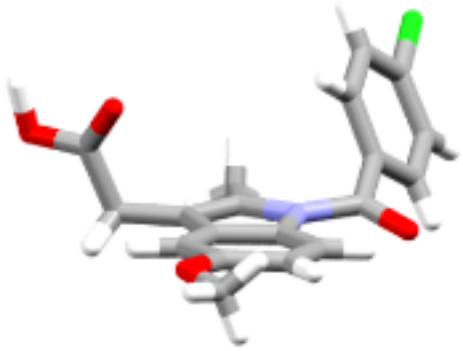

Minimized energies for optimized individual molecules and molecular pairs between IMC conformations, GLU and HIS

Compound	Minimized energy (kcal/mol)
trans-IMC	+50.29
cis-IMC	+51.64
GLU	-7.52
HIS	+21.54
trans-IMC:GLU	+18.77
cis-IMC:GLU	+20.47
trans-IMC :HIS	+52.65
cis-IMC :HIS	+47.98

Calculated association energies between different IMC conformations with GLU and HIS

Combination of compounds	ΔE (kcal/mol)
trans-IMC:GLU	-24.00
cis-IMC:GLU	-23.65
trans-IMC :HIS	-19.18
cis-IMC :HIS	-25.20

S11. Induction times - Effect of supersaturation on IMC polymorph distribution

supersaturation	Overall		γ-form		α-form	
	Induction time (min)	R^2	Induction time (min)	R^2	Induction time (min)	R^2
5	345	0.94	1111	0.96	555	0.84
5.5	200	0.93	1000	0.88	294	0.87
6	38	0.97	833	0.97	40	0.97
6.5	19	0.99	106	0.95	39	0.93
7	12	0.91	96	0.95	26	0.98

S12. Effect of solvent system

Polymorphic distribution

Solvent	Supersaturation	Condition	Percentage of vials crystallized in 24 hours	Polymorphic distribution in the crystallized vials			
				γ-form only	α-form only	Solvate	Mixture
Ethanol	6	Bulk	27.25%	51.37%	42.20%	N/A	6.43%
		With HIS	91.25%	20.54%	75.35%	N/A	4.11%
Acetone	2	Bulk	60%	0%	0%	100%	0%
		With HIS	82.5%	0%	0%	100%	0%
Methanol	6	Bulk	51.28%	2.5%	2.5%	97.5%	0%
		With HIS	73.41%	22.41%	0%	77.59%	0%
Ethyl acetate	6	Bulk	80%	78.09%	18.75%	0%	3.16%
		With HIS	97.5%	71.79%	24.35%	0%	3.84%
Eth:ace 1:1	2	Bulk	82.5%	67%	0%	33%	0%
		With HIS	23.75%	0%	0%	100%	0%

Induction time

Solvent	Supersaturation	Condition	Overall		γ-form		α-form	
			Induction time (min)	R^2	Induction time (min)	R^2	Induction time (min)	R^2
Ethanol	6	Bulk	322	0.90	434	0.95	1000	0.90
		With HIS	38	0.97	833	0.97	40	0.97
Acetone	2	Bulk	97	0.72	N/A	N/A	N/A	N/A
		With HIS	73	0.92	N/A	N/A	N/A	N/A
Methanol	6	Bulk	312	0.92	N/A	N/A	N/A	N/A
		With HIS	116	0.82	1250	0.92	N/A	N/A
Ethyl acetate	6	Bulk	17	0.92	19	0.89	435	0.77
		With HIS	40	0.81	58	0.71	175	0.75
Eth:ace 1:1	2	Bulk	82	0.99	117	0.96	N/A	N/A
		With HIS	666	0.91	N/A	N/A	N/A	N/A

S13. Raman Face indexing

Comparison of Raman spectra obtained for each family of faces between different crystals

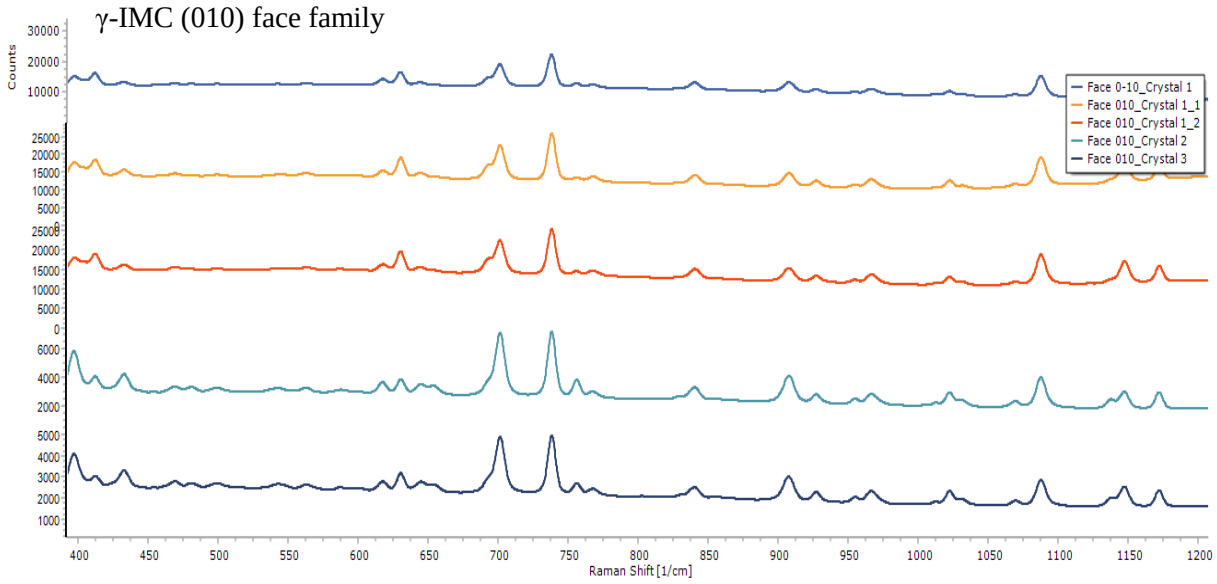

γ-IMC (100) face family

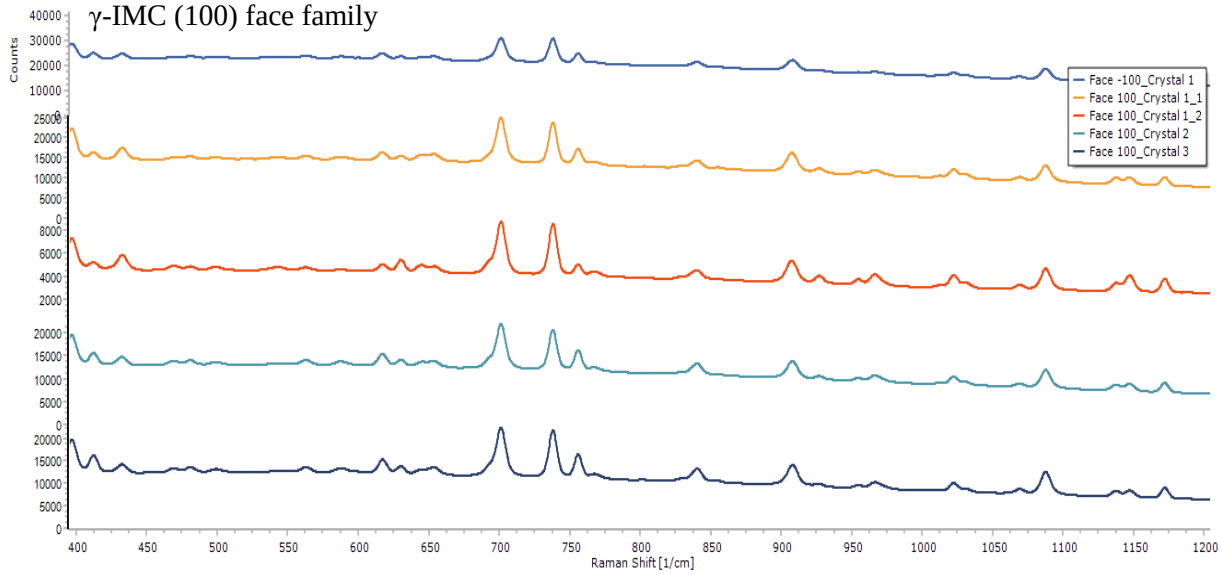

γ-IMC (001) face family

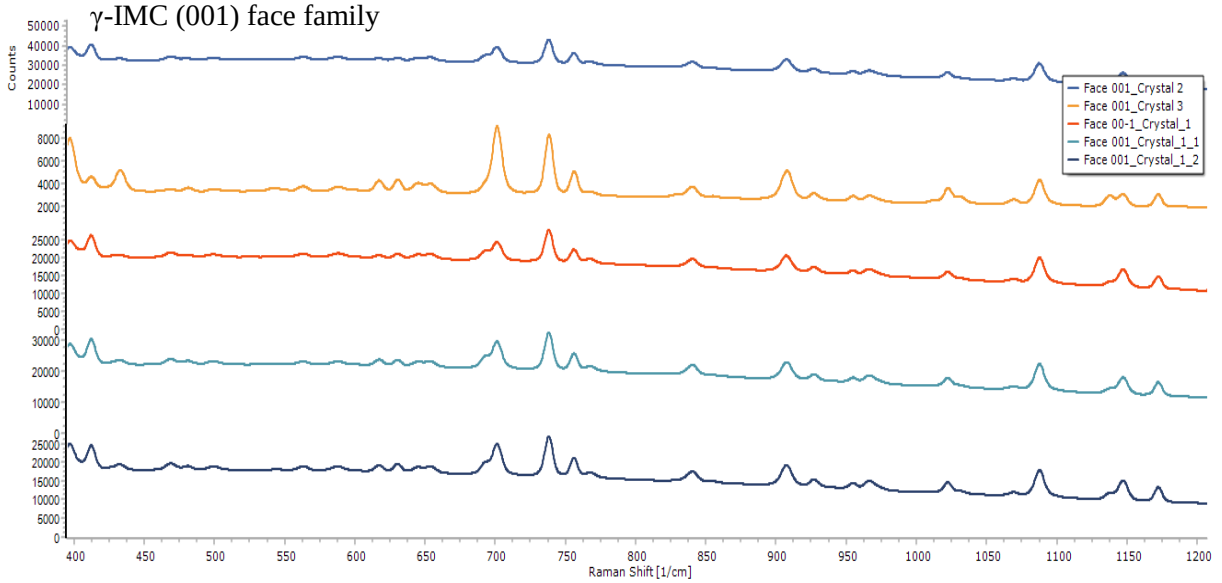

γ-IMC (-101) face family

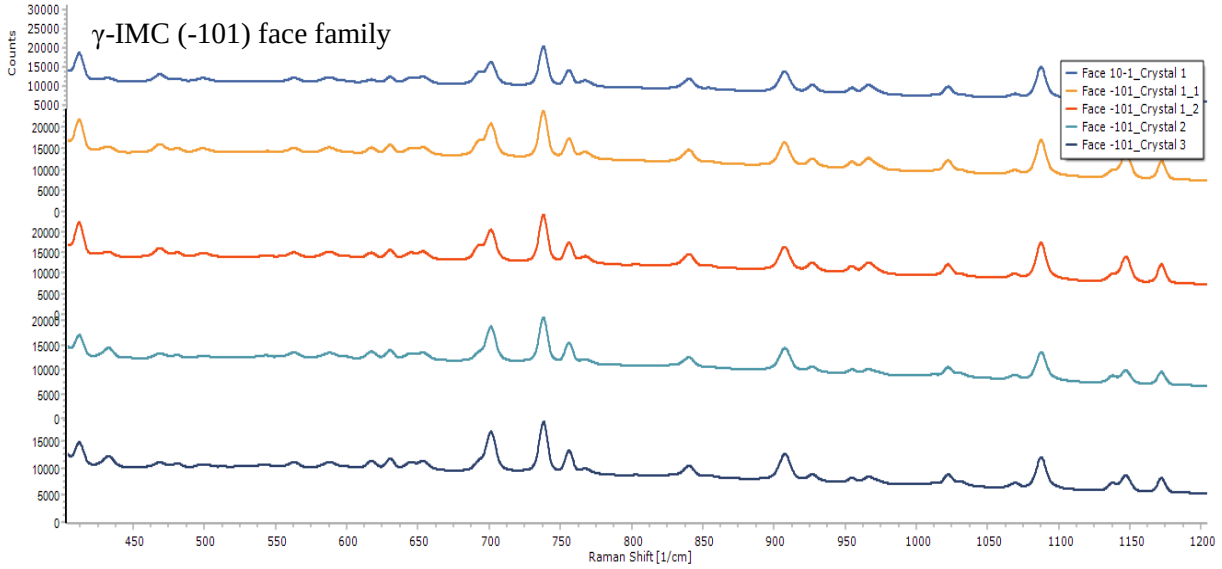

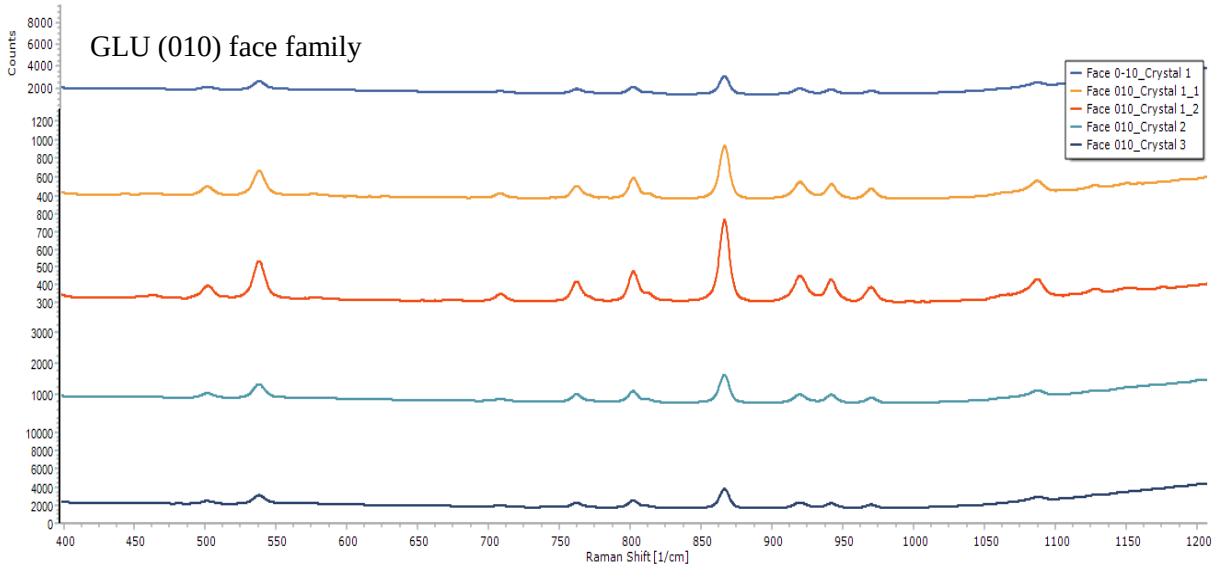
GLU (010) face family
Counts
Raman Shift [1/cm]
Face 0-10_Crystal 1
Face 010_Crystal 1_1
Face 010_Crystal 1_2
Face 010_Crystal 2
Face 010_Crystal 3

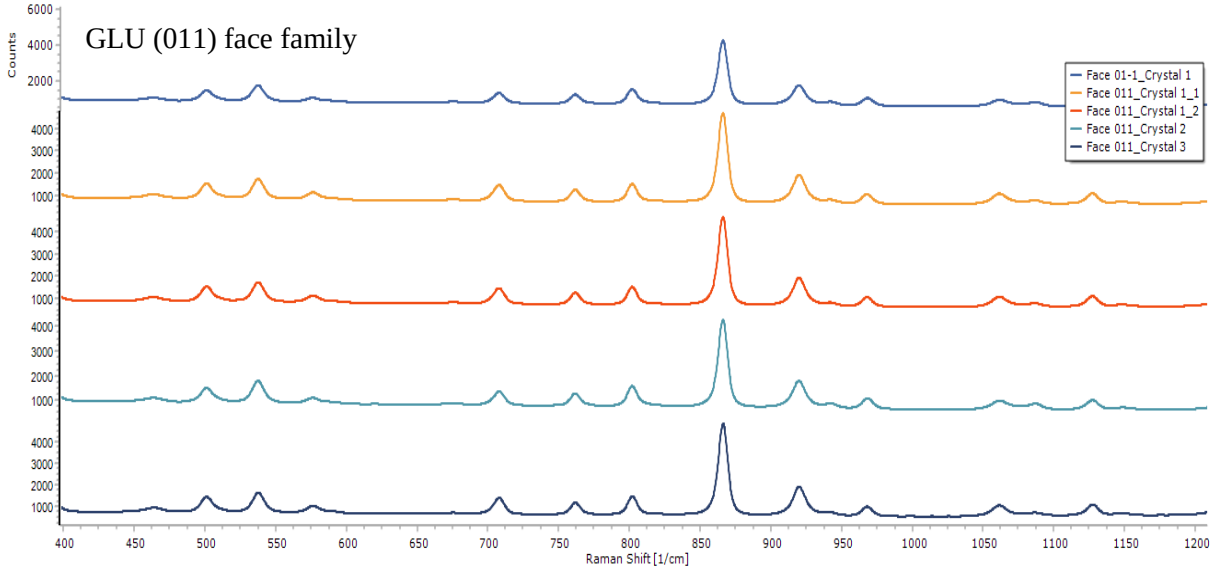
GLU (011) face family
Counts
Raman Shift [1/cm]
Face 01-1_Crystal 1
Face 011_Crystal 1_1
Face 011_Crystal 1_2
Face 011_Crystal 2
Face 011_Crystal 3

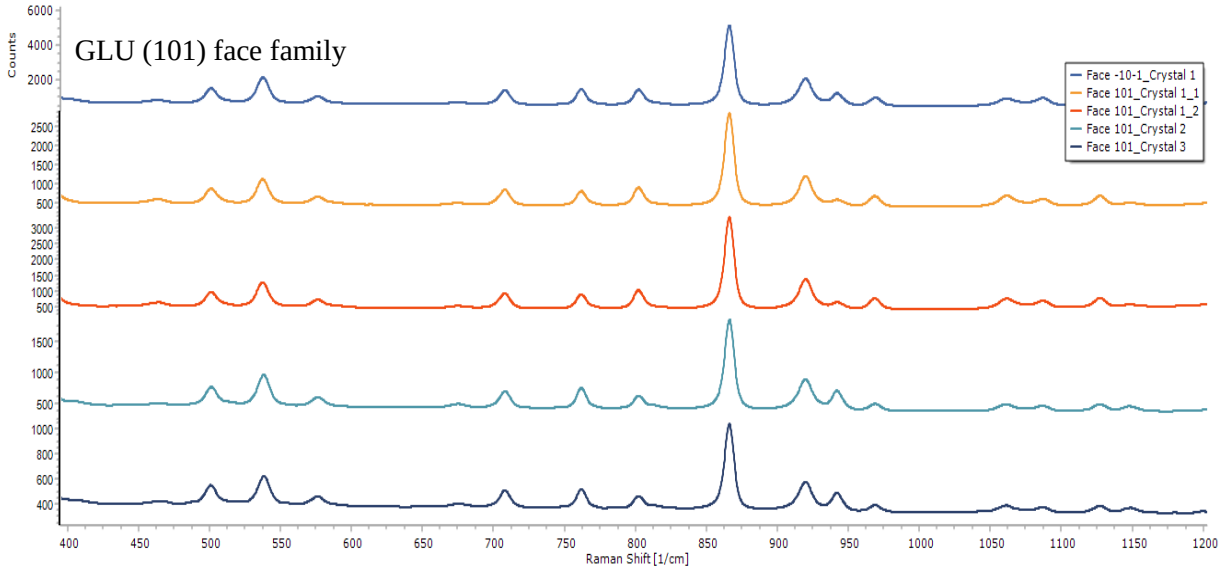
GLU (101) face family
Counts
Raman Shift [1/cm]
Face -10-1_Crystal 1
Face 101_Crystal 1_1
Face 101_Crystal 1_2
Face 101_Crystal 2
Face 101_Crystal 3

HIS (001) face family

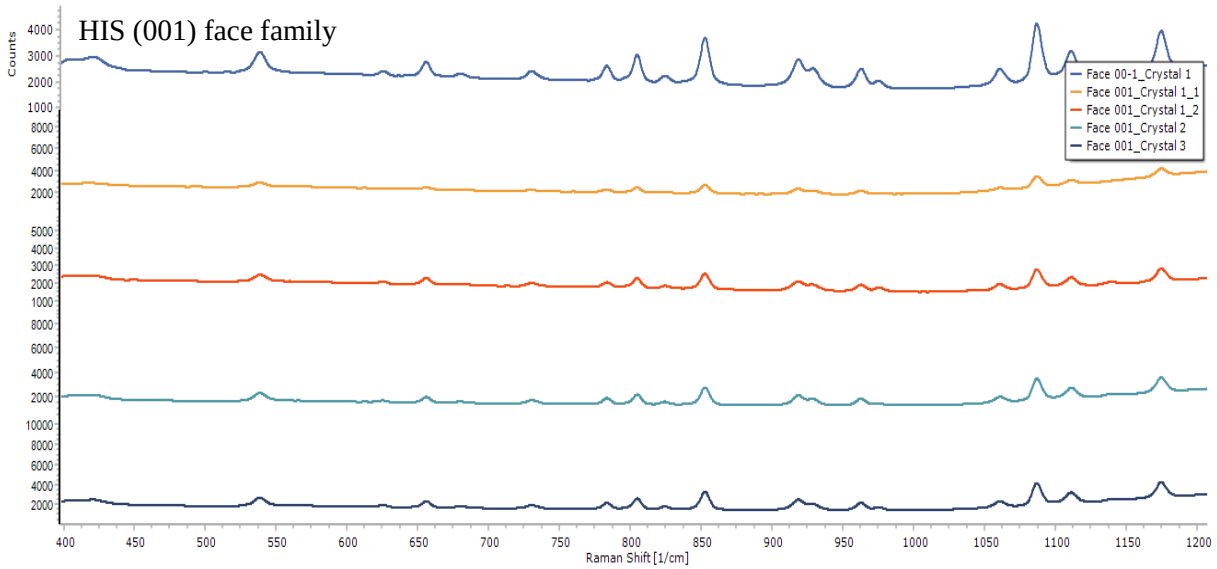

HIS (011) face family

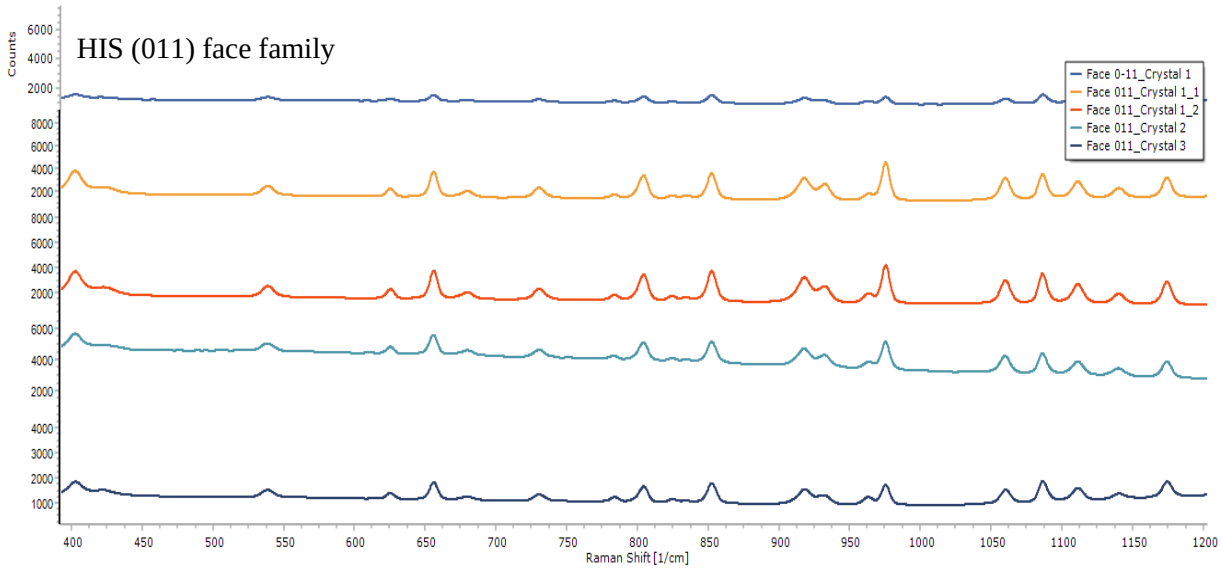

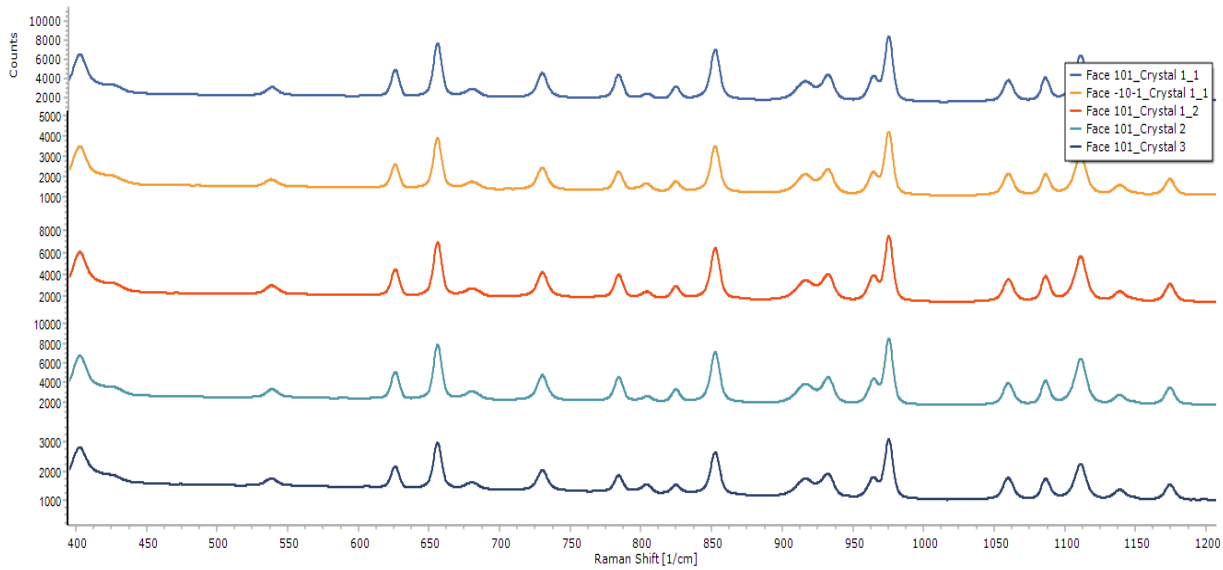

Unique distinguishable identifiers for each face family for each compound

Compound	Face family	Identifier description
γ-IMC	{101}	Peak at 412 is more intense than peak at 432 Peak at 630 is more intense than peak at 617 No peak at 653 Peak at 701 has a shoulder Peak at 756 is less intense than peak at 767 No peak at 1138
	{100}	Peak at 412 is less intense than peak at 432 Peak at 630 is less intense than peak at 617 Peak present at 653 Single peak at 701 without a shoulder Peak at 756 is more intense than peak at 767 Peak present at 1138
	{001}	Peak at 412 is less intense than peak at 432 Peak at 630 is almost equal in intensity to peak at 617 Peak present at 653 Single peak at 701 without a shoulder Peak at 756 is more intense than peak at 767 Peak present at 1138
	{-101}	Peak at 412 is more intense than peak at 432 Peak at 630 is more intense than peak at 617 Peak present at 653 Peak at 701 has a shoulder Peak at 756 is more intense than peak at 767 No peak at 1138
HIS	{001}	Peak at 783 is less intense than peak at 805 No peak at 834 Peak at 918 is more intense than peak at 932 Peak at 962 is more intense than peak at 975 Peak at 1087 is more intense than peaks at 1061 and 1111
	{011}	Peak at 783 is more intense than peak at 805 Peak present at 834 Peak at 918 is more intense than peak at 932 Peak at 962 is less intense than peak at 975 Peak at 1087 is more intense than peaks at 1061 and 1111
	{101}	Peak at 783 is more intense than peak at 805 No peak at 834 Peak at 918 is less intense than peak at 932 Peak at 962 is less intense than peak at 975 Peak at 1087 is less intense than peaks at 1061 and 1111
GLU	{010}	No peak at 576 Peak at 762 is more intense than peak at 708, less intense than peak at 802

		Peak at 942 is more intense than peak at 969 No peak at 1062
	{011}	Peak present at 576 Peak at 762 is less intense than peaks at 708 and 802 Peak at 942 is less intense than peak at 969 Peak present at 1062
	{101}	Peak present at 576 Peak at 762 is more intense than peaks at 708 and 802 Peak at 942 is more intense than peak at 969 Peak present at 1062

S14. Morphology prediction and analysis of surface functional groups

The exact surface area values are not available for experimentally analyzed crystals. Thus, in the following analysis, the faces are ranked according to the relative surface areas (highest to lowest) of experimentally analyzed crystals. For example, in the γ-IMC, for all the experimentally analyzed crystals, (010) family faces had the highest relative surface area (SI S6). The functional group analysis was conducted to a constant area of 20x20 $Å^2$ for a comparable analysis.

γ-IMC

Predicted faces	**Experimental faces (sorted in the order of surface area)**	**Available functional groups in 20x20 $Å^2$**
{ 0 1 0}	{ 0 1 0}	COOH (8), Cl (6), C=O (6), O-CH_3 (8)
{ 1 0 0}	{ 1 0 0}	COOH (8), Cl (6), C=O (6), O-CH_3 (6)
{ 1 0 -1}	{ 1 0 -1}	COOH (5), Cl (6), C=O (5), O-CH3 (6)
{ 0 0 1}	{ 0 0 1}	COOH (6), Cl (9), C=O (9), O-CH3 (6)
{ 1 1 1}	{ 1 1 1}	COOH (5), Cl (9), C=O (9), O-CH3 (6)
{ 0 1 1}	N/A	N/A
{ 1 1 0}	N/A	N/A
{ 1 0 1}	N/A	N/A
{ 1 1 -1}	N/A	N/A
{ 1 -1 -1}	N/A	N/A

N/A- did not observe in experimentally obtained crystals

{ 0 1 0}
COOH groups are exposed

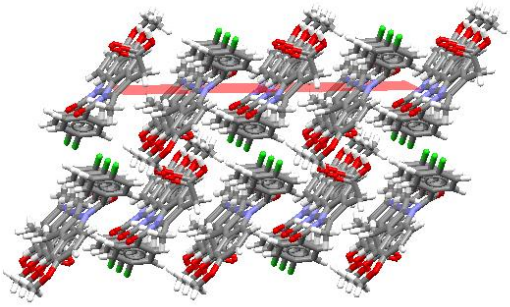

{ 1 0 0}
COOH groups are covered

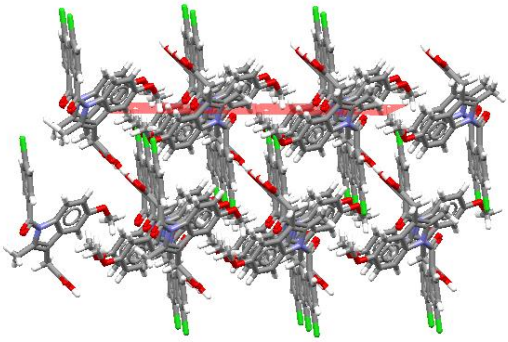

{ 1 0 -1}
COOH groups are exposed

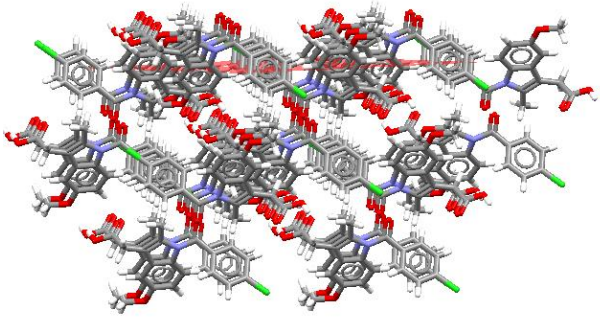

{ 0 0 1}
COOH groups are covered

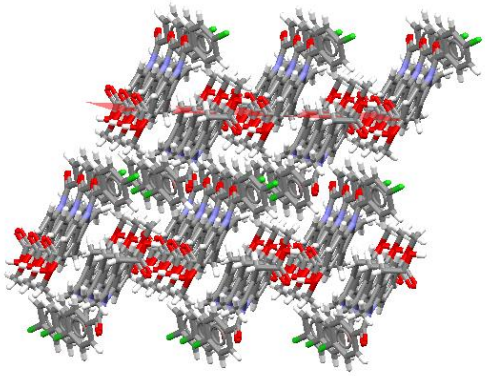

{ 1 1 1}
COOH groups are covered

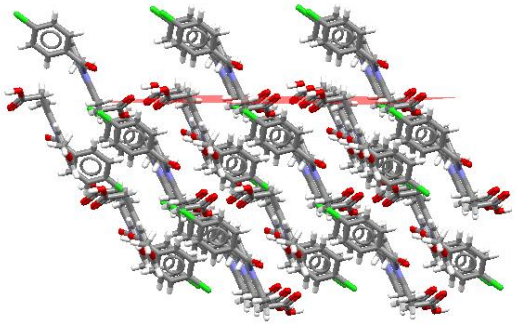

α-IMC

Predicted faces	Available functional groups in 20x20 Å^2
{ 0 0 1}	COOH (4), Cl (6), C=O (0), O-CH_3 (4)
{ 0 1 1}	COOH (5), Cl (0), C=O (8), O-CH_3 (4)
{ 0 -1 1}	COOH (0), Cl (17), C=O (9), O-CH_3 (4)
{ 0 2 0}	COOH (9), Cl (0), C=O (9), O-CH_3 (9)
{ 0 -2 0}	COOH (8), Cl (18), C=O (8), O-CH_3 (0)
{ 1 0 0}	COOH (4), Cl (4), C=O (4), O-CH_3 (5)
{ 1 1 -1}	COOH (6), Cl (3), C=O (5), O-CH_3 (6)
{ 1 -1 -1}	COOH (5), Cl (8), C=O (4), O-CH_3 (6)
{ 1 0 1}	COOH (4), Cl (5), C=O (3), O-CH_3 (4)

{ 0 0 1}

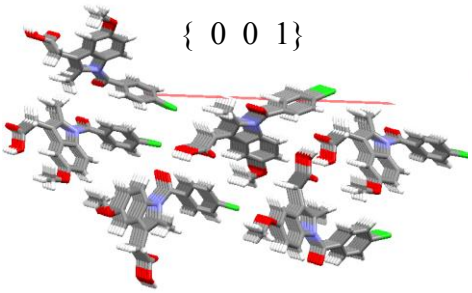

{ 0 1 1}

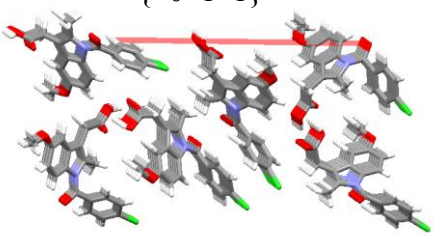

{ 0 -1 1}

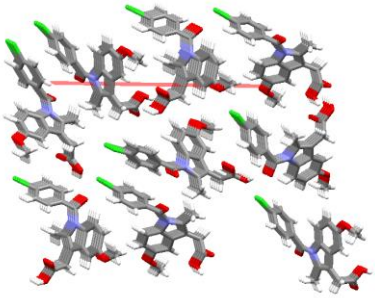

{ 0 2 0}

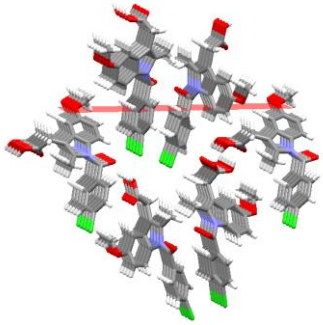

{ 0 -2 0}

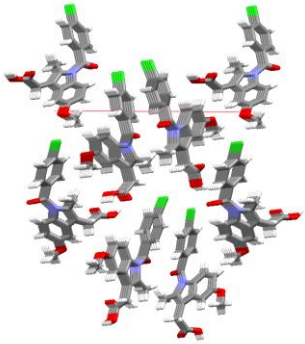

{ 1 0 0}

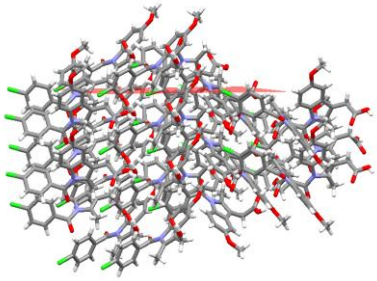

{ 1 1 -1}

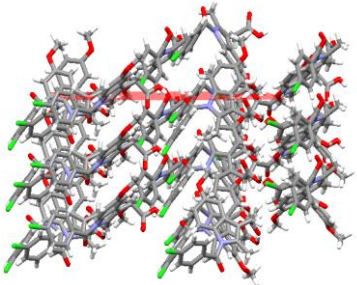

{ 1 -1 -1}

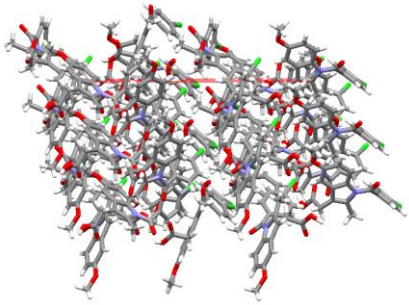

{ 1 0 1}

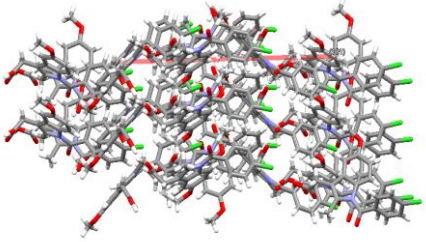

Predicted faces	Experimental faces (sorted in the order of surface area)	Available functional groups in 20x20 Å^2
{ 0 2 0}	{ 0 1 0}	COOH (9), COO^-(16)
{ 0 1 1}	{ 0 1 1}	COOH (5), COO^-(4)
{ 1 0 1}	{ 1 0 1}	COOH (3), COO^-(8)
{ 1 1 1}	{ 1 1 1}	COOH (5), COO^-(10)
{ 1 1 0}	N/A	N/A

N/A- did not observe in experimentally obtained crystals

{ 0 1 0}
COOH groups are exposed

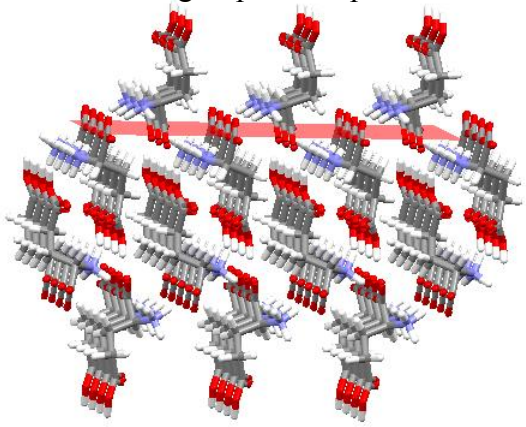

{ 0 1 1}
COOH groups are exposed

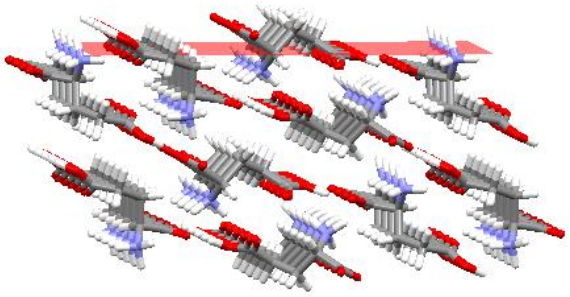

{ 1 0 1}
COOH groups are covered

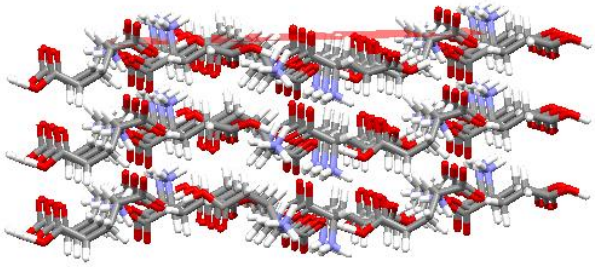

{ 1 1 1}
COOH groups are exposed

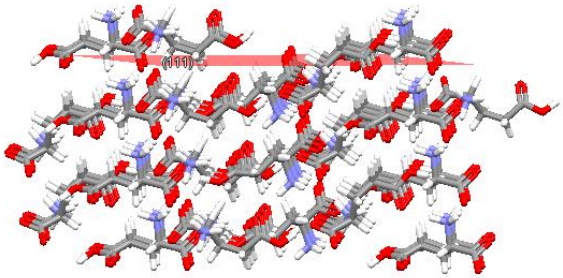

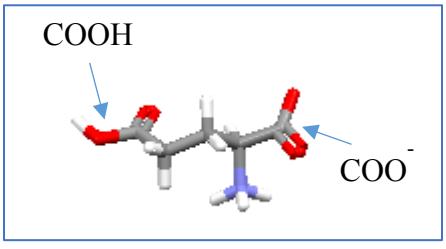

HIS

Predicted faces	Experimental faces (sorted in the order of surface area)	Available functional groups in 20x20 Å^2
{ 0 0 2}	{ 0 0 1}	COO^- (12), N_{imid}(12)
{ 0 1 1}	{ 0 1 1}	COO^- (5), N_{imid}(0)
{ 1 0 1}	{ 1 0 1}	COO^- (6), N_{imid}(7)
{ 1 1 1}	{ 1 1 1}	COO^- (8), N_{imid}(7)
{ 1 1 -1}	{ 1 1 -1}	COO^- (13), N_{imid}(3)
{ 1 1 0}	{ 1 1 0}	COO^- (10), N_{imid}(3)

{ 0 0 2}
COO- and N_{imid} groups are exposed

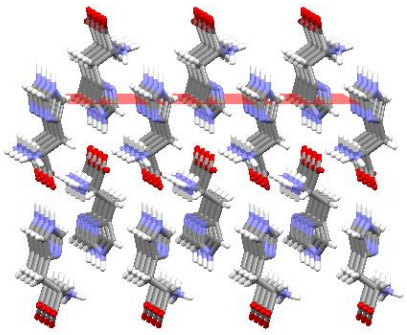

{ 0 1 1}
COO- and N_{imid} groups are exposed

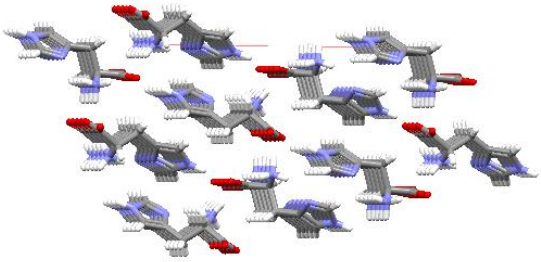

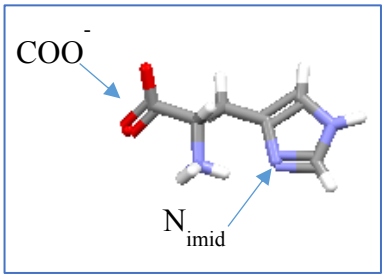

{ 1 0 1}
COO- and N_{imid} groups are exposed

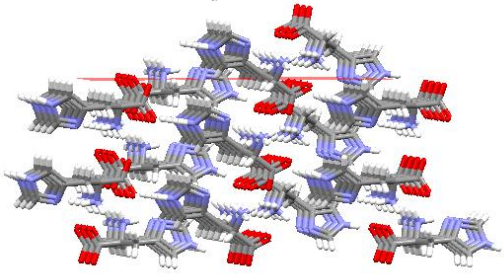

{ 1 1 1}
COO- and N_{imid} groups are exposed

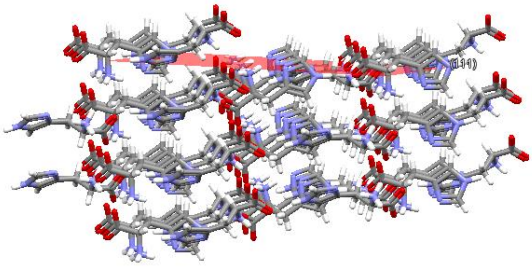

{ 1 1 -1}
COO- and N_{imid} groups are exposed

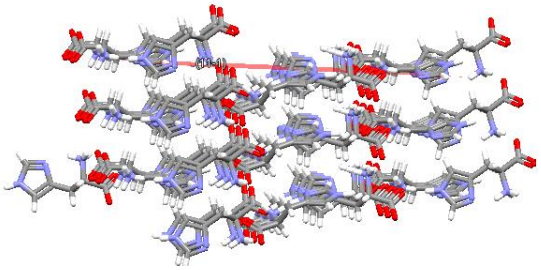

{ 1 1 0}
COO- and N_{imid} groups are exposed